On the determination of sound speeds in cubic crystals and isotropic media using a broadband ultrasonic point-source/point-receiver method

Kwang Yul Kim, Wolfgang Sachse and A. G. Every

Citation: The Journal of the Acoustical Society of America **93**, 1393 (1993); doi: 10.1121/1.405426
View online: https://doi.org/10.1121/1.405426
View Table of Contents: https://asa.scitation.org/toc/jas/93/3
Published by the Acoustical Society of America

On the determination of sound speeds in cubic crystals and isotropic media using a broadband ultrasonic point-source/point-receiver method

Kwang Yul Kim, Wolfgang Sachse, and A. G. Every[a)]
Department of Theoretical and Applied Mechanics, Cornell University, Ithaca, New York 14853

(Received 1 August 1990; revised 20 October 1992; accepted 20 October 1992)

This paper describes methods for determining the speeds of elastic waves propagating in cubic single crystals using a broadband point-source and point-receiver, i.e., PS/PR, technique in which transient ultrasonic pulses are simultaneously propagated over a broad angular range of directions in a specimen. Emphasis is given to determination of all three wave speeds from one detected waveform resulting from a single excitation pulse. First described is the determination of both longitudinal and shear wave speeds in an isotropic solid from the waveform detected by an arbitrarily located sensor. Then, measurements made in various directions in ⟨100⟩-, ⟨110⟩-, and ⟨111⟩-oriented silicon single crystal plates are analyzed. It is found that one obtains the most accurate determination of the three wave speeds from a single waveform detected by the sensors located in a {101}-type direction in both ⟨100⟩- and ⟨110⟩-oriented crystal specimens. It is found that a pointlike capacitive displacement sensor generally yields better results for the wave-speed measurements than a pointlike piezoelectric transducer.

PACS numbers: 43.35.Cg, 43.35.Yb

INTRODUCTION

There are many techniques that have been used for the measurement of the speed of propagation of sound in anisotropic media. These include ultrasonic plane-wave techniques which utilize specific transducers energized by broadband, narrow-band, or rf (radio frequency) burst pulse or continuous-wave (cw) excitations to generate longitudinal or shear waves in a specimen. With the pulse methods, the speed of sound is typically determined by sing-around,[1] double-pulse,[2] pulse-superposition,[3] or echo-overlap[4] techniques while the cw techniques are most commonly based on transmission measurements[5-7] or various forms of spectrometers.[8] These techniques and variations thereof are reviewed in a number of review articles and monographs, cf. Refs. 9–11. All of them are capable of detecting very small changes in wave speed, typically to better than one part in 10^5.

An recent alternative to the plane-wave technique is that utilizing the transient signals generated by a source of small aperture and detected by a small aperture, "point" receiving transducer. The apertures of both excitation source and detecting sensor are much smaller than the dominant wavelength of the generated signal and the source-to-receiver separation. This testing configuration has been called the point-source/point-receiver (PS/PR), technique.[12] The point source of known time characteristics generates signals which simultaneously propagate over a broad angular range of directions in a specimen where they are detected by a point receiver at an arbitrary receiver site. Although the resulting waveforms are more complex than plane-wave signals, the advantages of this method include its simplicity and the possibility for determining all the wave speeds of an elastic solid from the waveform resulting from a single excitation pulse. Other advantages include minimal surface preparation and the ability to test specimens of arbitrary geometry.

The transient elastic waves are generated on the surface of the specimen by broadband excitation sources which have included the fracture of a very small capillary[13] or a pencil lead,[14] the bombardment with radiation of very short duration pulses of high-intensity lasers,[15] electron beams,[16] or x rays.[17] A discussion of the requirements and operational characteristics of a number of sources and receivers which can be used as the basis of a PS/PR measurement system has been given.[18] When PS/PR signals are to be used for wave-speed measurements, the transient characteristic of these signals require that single-shot time interval counters be used or that the signals be recorded with a waveform digitizer for subsequent determination of the arrival times of various wave modes. Because waveform digitizers capable of sampling analog signals at GHz sampling rates are becoming available, it should become possible to determine wave speeds with increasingly higher resolution.

Examples of wave-speed measurements in isotropic materials made by the PS/PR technique were provided by the authors,[12,19] using the glass capillary fracture as a source and measuring the arrival times of the signals at epicenter with miniature piezoelectric detectors. Features of the PS/PR method related to wave-speed measurements in platelike specimens have been described by Hsu.[20] Measure-

[a)] Permanent address: University of the Witwatersrand, Johannesburg, South Africa.

 0001-4966/93/031393-14$06.00

ments using a high-intensity laser beam as a source and a laser interferometer as a sensor have been carried out by other investigators.[21–25] The advantage of the latter is that it utilizes a noncontact source and receiver, thus requiring no bond correction as is the case for piezoelectric transducers. Such measurements can also be made at high temperatures. However, the laser-based measurements suffer from a poor signal-to-noise ratio and thus usually require signal averaging to improve it. Furthermore, a high-intensity beam sometimes results in surface damage by ablation.

Recently, Aussel and Monchalin[21] have applied the laser beam technique to make wave-speed measurements in cubic single crystals of germanium of ⟨100⟩, ⟨110⟩, and ⟨111⟩ orientations. They used a combination of epicentral signals to determine the three elastic constants of germanium. More recently, Castagnède *et al.*[26–28] used waveform data obtained by scanning a laser beam over the surface of several anisotropic composite materials to determine all the elastic constants of the materials whose symmetry was higher than or equal to orthotropic.

In this paper, we describe methods of determining wave speeds from both epicentral and off-epicentral signals detected by suitably positioned sensors. Special emphasis is given to the determination of all the wave speeds pertaining to cubic and isotropic elastic solids from a single waveform measured in one particular source/receiver configuration. This provides for an expedient determination of wave speeds in various directions in a material and it also eliminates the errors associated with using crystal specimens of different orientations which may possess slightly different elastic moduli. It will be shown that this requires the determination of the arrivals of various wave-mode fronts including those corresponding to longitudinal and transverse waves, their multiple reflections from the free surfaces of the specimen, wave mode-converted signals as well as head-wave fronts.

Three optically polished silicon single-crystal disks of ⟨100⟩, ⟨110⟩, and ⟨111⟩ orientations, which were 7.62 cm in diameter and approximately 1.0 cm thick, were used as specimens. The testing geometry of these specimens is shown in Fig. 1(a)–(c). Plates of soda-lime glass and polycrystalline aluminum alloy 6061-T661 were used as elastically isotropic specimens. A glass capillary fracture, which is characterized as a vertical, monopolar Heaviside step force, with risetime less than 100 ns, was adopted as the excitation source principally because it generates much stronger signals when compared to those generated by a high-intensity laser pulse, which was also occasionally used to serve as a different mode of excitation. The signals were detected with either a capacitive displacement transducer of 1-mm aperture or a piezoelectric transducer with aperture of 1.3 mm. The former was principally used to detect the signals from the capillary source while the latter was used to detect signals from the capillary as well as the pulsed laser sources.

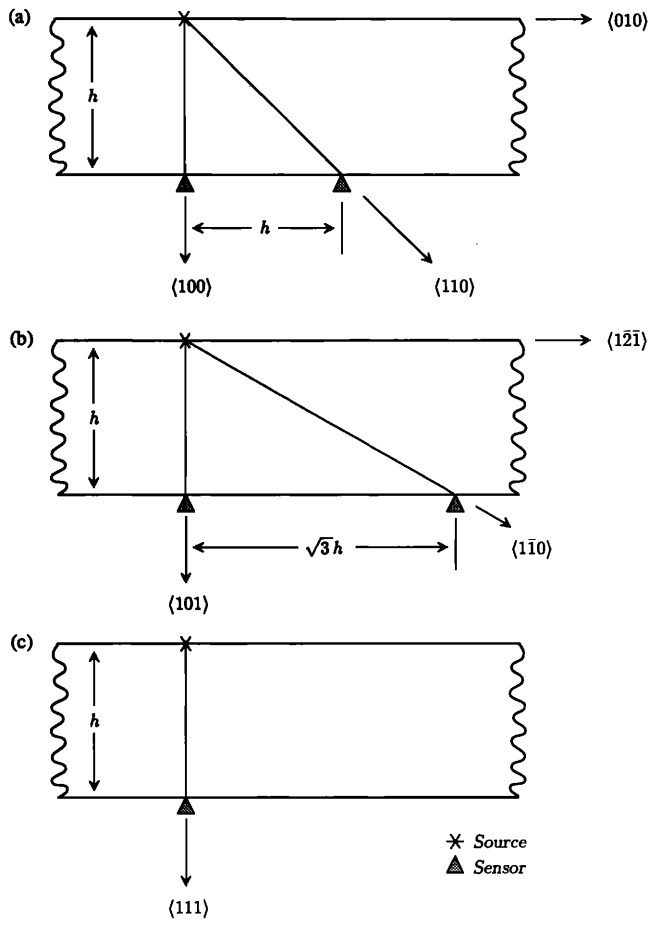

FIG. 1. Locations of excitation sources and sensors on the single-crystal specimens of silicon. (a) ⟨100⟩-oriented crystal. (b) ⟨101⟩-oriented crystal. (c) ⟨111⟩-oriented crystal.

I. THEORY

Considerable effort has been devoted to the calculation of transient waveforms from various excitation sources in isotropic, infinite elastic continua, half-spaces, and plates (cf. Ref. 29), and for propagation in epicentral[30] and near-field, off-epicentral directions of an isotropic, bounded plate of infinite dimensions.[31–34] Synthetic waveforms from monopolar and dipolar point sources as well as line forces have been computed. The source-time functions are typically a delta function, Heaviside step function, linear or parabolic ramp-step functions, among others. Viscoelastic dissipation effects of the medium have also been considered.[35,36] Such calculations have provided a catalog of ideal synthetic waveforms against which measured waveforms can be compared. Indeed, there is considerable agreement between the computed and measured waveforms, particularly with regard to the location of singularities and discontinuities in slope but in many cases also to the precise shape of the waveform.

Much less is known about the propagation of transient signals through a bounded anisotropic medium. The general form of the solution to the Cauchy problem has been provided by Duff.[37] The propagation of transient waves in infinite, transversely isotropic media has been analyzed by Cameron and Eason[38] and Buchwald[39] and asymptotic far-field solutions have been explored by Buchwald,[39] Yeats,[40] and Tverdoklebov and Rose.[41] The central idea emerging from these theoretical considerations is that singu-

larities and discontinuities in the wave field propagate on primary and secondary wave fronts. These wave fronts can be predicted from consideration of the wave or group velocity surface of the medium. However, to the authors' knowledge, there are, as yet, no published waveforms that can be used for comparison with our measured signals.

For isotropic media and in the absence of dispersion, the group and phase velocity surfaces coincide, but for anisotropic media these two surfaces are usually distinct from each other. However, as we will see, in certain high symmetry directions, they may again coincide. The shape of the group velocity surface is, in general, much more complex than that of the phase velocity surface.[37,42] Depending on the material's symmetry and the degree of anisotropy, it is not unusual that the former will contain cuspidal edges where the surface folds back on itself. Within these folded regions, there are multiple group velocities in each direction and for a particular wave branch. This must be borne in mind when interpreting transient waveforms. At the same time it should be remarked that in cases when the degree of anisotropy is low, the phase and group velocities lie close to each other and their difference may be less than the experimental error involved in their determination. Thus existing elastic constant data derived on the basis of phase velocity considerations,[26-28] where it might be argued that the group velocity should have been used are not necessarily invalidated. At the very least, they can be regarded as approximate fits to experimental data. Indeed, because of the mathematical complexity of the group velocity surface and the indirect procedure that is required to determine the elastic constants by matching group velocities, there is some merit to using a fit to phase velocities as a logical step in a procedure for limiting the parameter domain.

The experimental results that we present below for silicon pertain to waves propagating in or close to the three high symmetry directions, {100}, {110}, and {111}. With the exception of transverse waves propagating in a {111}-type direction, waves whose normals lie in these high symmetry directions also have group velocities in the same directions and the phase and group velocities coincide. Thus we are able to make use of the simple formulas that exist for phase velocities in these directions to extract elastic constants from our signals. However, because of the complex folding of the wave surface, there are also waves whose normals lie well away from the high symmetry directions but that have ray vectors lying in these symmetry directions. These oblique waves are present in some of our waveforms and, therefore, our interpretation in the following section must be broadened to take them into account.

A solid of cubic symmetry is characterized by three independent elastic constants C_{11}, C_{12}, and C_{44} (see Ref. 43). The elastic wave equation for such a medium admits plane-wave solutions which are governed by the Christoffel equation,[44-46]

$$(\Gamma_{rs} - \rho V^2 \delta_{rs}) U_s = 0, \tag{1}$$

where

$$\Gamma_{rs} = \begin{cases} (C_{12} + C_{44}) n_r n_s & (r \neq s) \\ C_{11} n_r^2 + C_{44}(n^2 - n_r^2) & (r = s) \end{cases} \tag{2}$$

is the Christoffel tensor, $\mathbf{n} = (n_r)$ is the wave normal, ρ is the density of the medium, V is the phase velocity, and $\mathbf{U} = (U_s)$ is the polarization vector of the wave. The components of the polarization vector $\mathbf{U}$ correspond to the eigenvectors of Γ_{rs}, and the corresponding eigenvalues ρV^2 are determined by the secular equation

$$|\Gamma_{rs} - \rho V^2 \delta_{rs}| = 0. \tag{3}$$

Expanding this determinant yields a cubic equation for V^2, whose solutions can be conveniently expressed in closed form in terms of trigonometric functions.[47,48] There are three solutions, one corresponding to quasilongitudinal waves and the other two to quasitransverse waves.

In the symmetry planes, one of the modes is pure transverse with polarization normal to the plane and the other two modes have polarization vectors lying in the plane. The secular equation in this case factorizes into a linear and a quadratic equation in V^2 and the resulting solutions can be easily inverted to recover the elastic constants from phase velocity data.

For $\mathbf{n}$ lying in the (001) plane at an angle of ϕ with the ⟨100⟩ direction, the three phase velocities are given by

$$\rho V_{s1}^2 = C_{44}, \tag{4}$$

for the pure shear mode, and

$$\rho V_l^2 = \tfrac{1}{2}\{(C_{11} + C_{44}) + [(C_{11} - C_{44})^2 + 4(C_{11} - C_s')(C_{44} - C_s')\sin^2 2\phi]^{1/2}\}, \tag{5}$$

for the quasilongitudinal, and

$$\rho V_{s2}^2 = \tfrac{1}{2}\{(C_{11} + C_{44}) - [(C_{11} - C_{44})^2 + 4(C_{11} - C_s')(C_{44} - C_s')\sin^2 2\phi]^{1/2}\}, \tag{6}$$

for the quasishear waves, where $C_s' \equiv (C_{11} - C_{12})/2$. The calculated directional dependence of these velocities in silicon using the elastic constants $C_{11} = 165.7$ GPa, $C_{44} = 79.56$ GPa, and $C_s' = 50.9$ GPa and a density of $\rho = 2332$ kg/m^3 is shown in Fig. 2.

For $\mathbf{n}$ lying in the $(1\bar{1}0)$ plane and making an angle φ with the ⟨001⟩ direction, the three phase velocities are given by

$$\rho V_{s1}^2 = C_{44} \cos^2 \varphi + C_s' \sin^2 \varphi, \tag{7}$$

for the pure shear mode and

$$\rho V_l^2 = \tfrac{1}{2}\{D_+ + [D_-^2 + (C_{44} - C_s') \times (3C_{11} + C_{44} - 4C_s')\sin^2 2\varphi]^{1/2}\}, \tag{8}$$

$$\rho V_{s2}^2 = \tfrac{1}{2}\{D_+ - [D_-^2 + (C_{44} - C_s') \times (3C_{11} + C_{44} - 4C_s')\sin^2 2\varphi]^{1/2}\}, \tag{9}$$

for the quasilongitudinal and quasitransverse waves, respectively, where

$$D_\pm \equiv (C_{11} \pm C_{44}) + (C_{44} - C_s')\sin^2 \varphi. \tag{10}$$

The calculated directional dependence of these velocities for silicon is shown in Fig. 3.

Further simplification occurs when $\mathbf{n}$ also lies along an axis of rotational symmetry. For $\mathbf{n}$ in a {100}-type direction, setting $\phi = 0°$, Eqs. (4)–(6) yield

$$\rho V_l^2 = C_{11} \tag{11a}$$

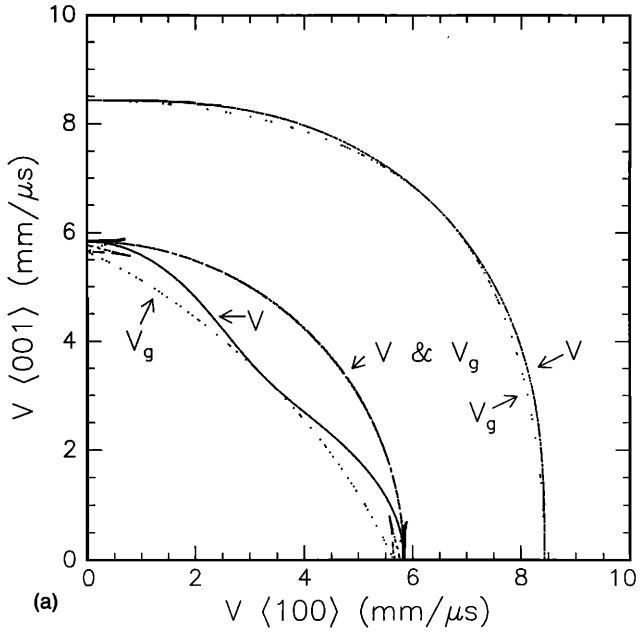

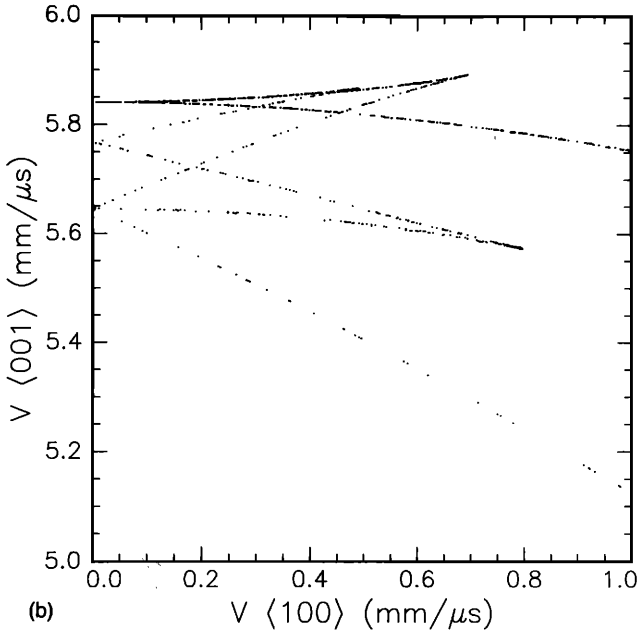

FIG. 2. (a) (001) sections of phase and group velocity surfaces of silicon. (b) Expanded view of group velocities close to the ⟨001⟩ direction.

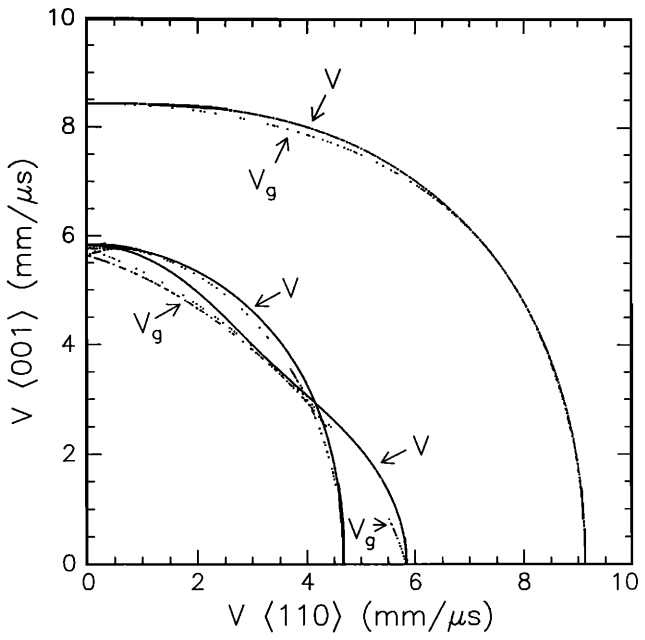

FIG. 3. (110) sections of phase and group velocity surfaces of silicon.

and

$$\rho V_{s1}^2 = \rho V_{s2}^2 = \rho V_s^2 = C_{44}. \tag{11b}$$

This is a pure mode direction in which the one mode is pure longitudinal and the other two, which are degenerate, are pure transverse. This degeneracy of two modes also defines the ⟨100⟩ direction to be an acoustic axis.[49–51] For **n** along a {110}-type direction, we set $\varphi = 90°$, then Eqs. (7)–(10) yield

$$\rho V_l^2 = C_{11} + C_{44} - C_s', \tag{12a}$$

$$\rho V_{s1}^2 = \rho V_s'^2 = C_s', \tag{12b}$$

$$\rho V_s^2 = \rho V_s^2 = C_{44}. \tag{12c}$$

These are also pure longitudinal and pure transverse wave modes, but the three velocities are distinct and so this is not an acoustic axis. For **n** along a ⟨111⟩ direction, setting $\cos\varphi = 1/\sqrt{3}$ in Eqs. (7)–(10) yields the velocities

$$\rho V_l^2 = C_{11} + \tfrac{4}{3}(C_{44} - C_s') \tag{13a}$$

and

$$\rho V_{s1}^2 = \rho V_{s2}^2 = (C_{44} + 2C_s')/3. \tag{13b}$$

Thus, the ⟨111⟩ is a pure mode direction as well as an acoustic axis. The above relations between elastic constants and phase velocities for waves propagating along the symmetry directions in a material of cubic symmetry are summarized in Table I.

For waves propagating in $\langle n_1, n_2, n_1 + n_2\rangle$-type directions lying in the $(11\bar{1})$ plane [see Fig. 1(b)], the Christoffel secular equation takes the form

$$(\rho V^2 - C_{44})(\rho V^2 - C_{11} - C_{44} + C_s')(\rho V^2 - C_s') - 4n_{12}^2(n_{12} + \tfrac{1}{2})(C_{44} - C_s')^2(3C_{11} + C_{44} - 4C_s') = 0, \tag{14}$$

where $n_{12}^2 \equiv n_1 n_2$. This is not a symmetry plane and Eq. (14) does not factorize but it can be solved numerically. The three solutions generally correspond to one quasilongitudinal and two quasishear modes.

In measurements of the elastic constants of cubic crystals with plane waves, there is overwhelming emphasis on velocity measurements in the three high symmetry directions. Apart from the simplicity of the inversion of the appropriate formulas to recover the C_{ij}'s, there are also practical considerations related to the mechanism of excitation, mode conversion, beam drift and sample preparation, etc. Some of these advantages carry over to the PS/PR technique, but in the latter technique, close attention must be given to the propagation of energy through the specimen.

TABLE I. Relations between elastic constants and phase velocities for materials of cubic symmetry.

Propagation direction	Direction of particle motion	Type of wave mode	Relation[a]
⟨100⟩	⟨100⟩	longitudinal	$\rho V_l^2 = C_{11}$
⟨100⟩	in plane (100)	shear	$\rho V_s^2 = C_{44}$
⟨110⟩	⟨110⟩	longitudinal	$\rho V_l^2 = C_{11} + C_{44} - C_s'$
⟨110⟩	⟨001⟩	shear	$\rho V_s^2 = C_{44}$
⟨110⟩	⟨1$\bar{1}$0⟩	shear	$\rho V_l^2 = C_s'$
⟨111⟩	⟨111⟩	longitudinal	$\rho V_l^2 = C_{11} + 4(C_{44} - C_s')/3$
⟨111⟩	in plane (111)	shear	$\rho V_s^2 = (C_{44} + 2C_s')$

[a] Where $C_s' \equiv (C_{11} - C_{12})/2$.

Unlike a plane-wave transducer, a point source injects energy into the material not via a single wave whose normal is perpendicular to the surface, but into all the propagating modes of the system including bulk waves, head waves, and surface waves, etc., even though our attention here is restricted principally to bulk waves. The energy of a plane wave of normal $\mathbf{n}$ and phase velocity $V(\mathbf{n})$ is propagated through the medium at the group velocity $\mathbf{V}_g$ given by

$$\mathbf{V}_g = (V - \mathbf{n}\cdot\nabla_{\mathbf{n}} V)\mathbf{n} + \nabla_{\mathbf{n}} V. \tag{15}$$

In our calculations, we have evaluated $\nabla_{\mathbf{n}} V$ by using an implicit differentiation of the Christoffel characteristic equation. For any given wave

$$\mathbf{V}_g \cdot \mathbf{n} = V, \tag{16}$$

which implies that when $\mathbf{V}_g$ is parallel to $\mathbf{n}$, the group and phase velocities are equal. This is the case for longitudinal and shear waves in the {100}- and {110}-type directions and with longitudinal waves propagating in the {111}-type directions. The measurement of these group velocities therefore readily yields the C_{ij}'s. For $\mathbf{n}$ away from a symmetry direction, $\mathbf{V}_g$ is, in general, not parallel to $\mathbf{n}$ and therefore the phase and group velocities are not equivalent. The angular separation between the rays of the two velocities can range up to 20° or more in a material, depending on the degree of anisotropy and propagation direction.

With the exception of certain special cases, there is no simple analytical formula available that yields the group velocity for a given arbitrary direction relative to the material's axes. Since the equation of the wave surface could be of degree as high as 150 (see Ref. 37), it is unlikely that a convenient closed-form solution to this problem will be readily forthcoming. There is the option of numerical methods for obtaining $\mathbf{n}$ and $\mathbf{V}_g$ but considerable care must be exercised to be certain of locating all collinear $\mathbf{V}_g$'s. We have made use of a Monté Carlo method to generate a large number of randomly directed $\mathbf{n}$'s and then sorted the associated ray vectors into a grid of directions. Figure 2 shows a (010) section of the wave surface of silicon which has been calculated in this way while Fig. 3 shows a (1$\bar{1}$0) section. Each point represents a ray vector which lies within 0.05° of the plane. For comparison, the phase velocities in the plane are also shown.

It is seen that the longitudinal sheet of the wave surface is the simplest of the three. It possesses no cuspidal edges and so there are no multiple velocities. The rays in this section are all associated with $\mathbf{n}$'s lying in the plane and the effect of anisotropy is simply to effect a tilting of $\mathbf{V}_g$ with respect to $\mathbf{n}$ in the plane.

The longitudinal phase and group velocities in the three principal directions coincide and the signal arrival time can be simply interpreted in terms of the material's elastic constants via Eqs. (11a), (12a), and (13a). Along most nonprincipal directions, the longitudinal phase and group velocities differ by $\lesssim 1\%$. Therefore, in our interpretation of experimental results for directions fairly close to the ⟨100⟩ direction, we have used the phase velocity formula for the longitudinal velocity. The error incurred thereby is less than the sum of the experimental uncertainties.

For the transverse modes, the difference between the phase and group velocities is much larger, ranging up to about 10% in some directions, hence, it is important to make the distinction. Both sheets of the two transverse modes exhibit cuspidal features. This is most pronounced for the slow transverse sheet near the ⟨001⟩ direction. Some of these edges are associated with in-plane $\mathbf{n}$'s where a reversal in the tilting of $\mathbf{V}_g$ occurs. Others are associated with folds in the wave surface that occur across the symmetry plane and which map an $\mathbf{n}$ on one side of the plane to a $\mathbf{V}_g$ on the other. One peculiar consequence of this folding is that some portions of the slow transverse sheet penetrate out beyond the fast transverse sheet, so that the distinction between slow and fast transverse becomes somewhat blurred. Of importance in the interpretation of our experimental results is the fact that in the ⟨001⟩ direction there are several group velocities. Taking also into account the fact that the receiver has a finite aperture, it is apparent that there is not just one transverse signal velocity, but rather, a range of velocities. This will be discussed further below. The highest group velocity in the ⟨001⟩ direction belongs to waves with $\mathbf{n}$ lying along this axis, so the earliest arrival time of the signal in this direction can be directly related to C_{44}.

In a {110}-type direction, the fast and slow transverse waves are well separated in their arrival. The slow transverse branch possesses no cuspidal features in this region and the phase and group velocities are parallel hence the signal arrival time yields C_s'. The fast transverse branch possesses a small cuspidal feature but the corresponding velocity spread

is $\lesssim 1\%$ for the detector used to make the measurements to be described and hence the signal arrival time can be simply related to C_{44}.

The propagation of transverse waves in a {111}-type direction is more complicated because a conical degeneracy of the two transverse branches occurs here. A transverse wave with **n** parallel to ⟨111⟩ does not have a single ray vector but rather a circular cone of ray vectors which disperse the energy of this wave away from the ⟨111⟩ direction in an effect known as *internal conical refraction*.[45,46] Nevertheless, inspection of Fig. 3 reveals that there is a marked concentration of transverse ray vectors in the ⟨111⟩ direction. This is borne out in the experimental results which we will describe later, in which there is a clear indication of a transverse wave signal in that direction. This is accounted for by folding in the slow transverse sheet of the wave surface which maps the ray vectors for six widely separated **n**'s into the ⟨111⟩ direction. Even though these **n**'s lie in symmetry planes, the corresponding velocities cannot be expressed in a simple way in terms of the material's elastic constants. Our measurements on silicon yield a value of ρV_s^2 close to $(C_{44} + 2C_s')/3$, which is predicted for the phase velocity in this direction, but this is not expected to be true for all materials.

We compare in the next paragraphs the information that can be extracted from the signals which have propagated in various directions in specimens of different orientations. Corresponding to the epicentral rays in a ⟨100⟩-oriented crystal are only two relations for the phase velocities and therefore determination of all three wave speeds is not possible with them. Of particular interest for determining the three phase velocities among the rays propagating in off-epicentral directions is that of a {110}-type direction because associated with this direction are one purely longitudinal and two purely transverse modes whose distinct phase velocities are given by Eqs. (12a)–(12c).

Also of importance are longitudinal rays that have undergone multiple reflections in propagating from the source located on the top surface of the specimen to the detector located in a {110}-type direction on the bottom surface, as depicted in Fig. 1(a). These rays are more easily identifiable than other types of multiply reflected or mode-converted rays. The directions of rays with an initial angle ϕ are crystallographically equivalent before and after reflection and the incident and reflection angles associated with such longitudinal rays are both equal to ϕ. If one can identify in a single waveform the arrivals of the first purely longitudinal mode, the two purely transverse modes, and some of multiply reflected longitudinal rays, it is possible to determine from the differences of these arrival times, three wave speeds by using Eqs. (12a)–(12c) and Eq. (5). In principle, it is possible to make use of a signal detected by the sensor of any direction ϕ, but the determination of the wave speeds using Eqs. (4)–(6) is far more complicated. For the reasons mentioned earlier, of particular interest is the determination of the three wave speeds with a ⟨101⟩-oriented crystal using an ⟨101⟩-directional epicentral ray and an off-epicentral signal detected by a sensor positioned in a ⟨1$\bar{1}$0⟩ direction from the excitation source on the surface opposite to the source. This testing

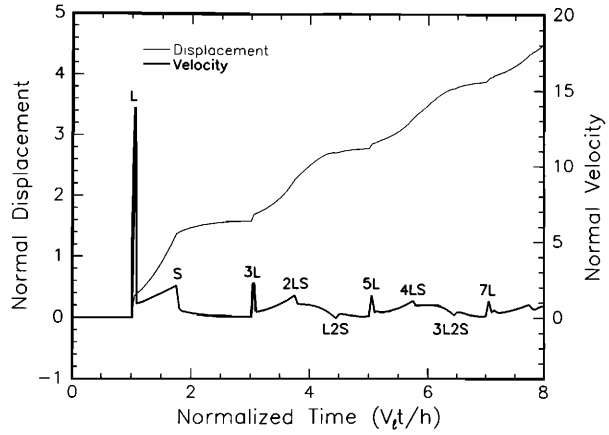

FIG. 4. Theoretical, normal responses at epicenter due to a vertical single force of Heaviside-step and impulse functions.

configuration is illustrated in Fig. 1(b).

The case of isotropic solids is far simpler. It is well known that the two elastic moduli of an isotropic solid, the Lamé constants, λ and μ, are related to the longitudinal and shear wave speeds by: $\rho V_s^2 = C_{44} = C_s' = \mu$ (pure transverse mode) and $\rho V_l^2 = C_{11} = \lambda + 2\mu$ (pure longitudinal mode).

The calculated normal displacement signal and impulse response (or *Green's function*) at epicenter resulting from a vertical, monopolar Heaviside step excitation are shown in Fig. 4. These data were generated using $V_l/V_s = 1.7$ and a plate specimen of thickness h. Similar theoretical curves but with $V_l/V_s = 2$ and a horizontal dipole source on the surface with the receiver located a distance of $2h$ away from the epicenter are shown in Fig. 5. In both these figures, the abscissa is expressed in units of normalized time, equal to $V_l t/h$, and the ordinate represents the signal magnitude in arbitrary units. Here, L, S and H denote, respectively, the longitudinal, shear, and head wave arrivals, and $mLnS$ represents the arrival of a ray which, through mode conversion at the surface, travels m times in the longitudinal mode and n

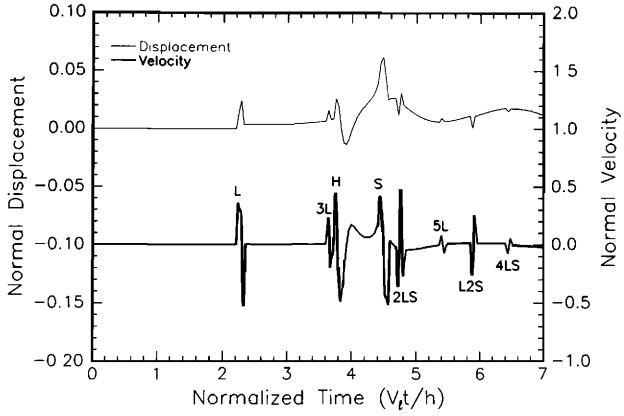

FIG. 5. Theoretical, normal responses at $2h$ units away from epicenter due to a horizontal dipole force of Heaviside-step and impulse functions of time.

times in the shear mode in propagating from the source to the receiver. If the instant of source excitation is unknown, one needs to identify in the detected waveform the arrivals of at least three modes in order to determine the two wave speeds V_l and V_s. This is the case when a glass capillary fracture is the excitation. Otherwise identification of two different wave mode arrivals suffices. The determination of both V_l and V_s is straightforward from an epicentral signal. However, for off-epicentral signals, one may need to identify and to determine the arrivals not only of the L and S modes but also the $3L$, $5L$,..., nL, $2LS$, $L\,2S$, and head wave modes, and so on, with the corresponding arrivals denoted by t_l, t_s, t_{3l}, t_{5l},..., t_{nl}, t_{2ls}, t_{l2s}, and t_h, where the subscript n is a positive odd integer.

II. EXPERIMENTAL DATA AND RESULTS

An excitation source of a vertical single force whose time evolution is a Heaviside step function with risetime less than 100 ns was generated by breaking a glass capillary of 80 μm OD$\times$50 μm ID with a razor blade on the surface of a specimen. Irradiation with a high intensity Nd:YAG laser pulse of 4-ns duration on the surface of a specimen was also used as a source resembling a horizontal dipole evolving as a Heaviside step function in time. The elastic waves generated by these sources propagate in a broad angular range of directions. Detection of the ultrasonic signals was at a particular location either by a capacitive displacement sensor whose circular sensing area was 1 mm in diameter or by a piezoelectric transducer having an active sensing element of 1.3-mm diameter. The general profile of the signal detected by the piezoelectric sensor was found to bear some resemblance to a normal velocity signal that was obtained by differentiating the displacement normal to the surface with respect to time. The signals detected by these sensors were amplified by a charge amplifier of bandwidth of 10 kHz to 10 MHz for the case of the capacitive sensor and by a preamplifier with bandwidth of 100 kHz to 20 MHz for the case of the piezoelectric transducer. The amplified signals were input to waveform recorders for digitization at a rate of 60 MHz with 10-bit resolution. The data in the memory of the digitizer could be transferred to a minicomputer for storage and subsequent processing. Additional details of the measurement system has been described previously.[52,53]

The following criteria were adopted for the identification of the arrivals of various modes in the detected signals: (i) The arrival of a particular mode is characterized as a step or a sudden change of shape in the displacement signal and as a sharp positive or negative peak in the velocity signal. (ii) The first arrival is always the longitudinal (L) mode and the arrivals of this and the multiply reflected longitudinal modes, i.e., ($3L$,$5L$,$7L$,...), are regularly spaced in the epicentral signal. (iii) For most engineering materials, Poisson's ratio lies between 0.1 and 0.4, corresponding to V_s/V_l ranging between 0.4 and 0.67. For epicentral and near-epicentral signals, the L mode is followed by shear modes which may include fast shear (S) and slow shear (S') modes. In the epicentral waveforms, these shear modes are followed by a $3L$ mode and then the $2LS$, $2LS'$, $L\,2S$, and $L\,2S'$ modes whose arrivals may or may not appear as pronounced features, depending on the efficiency of the mode conversion. (vi) In the velocity signal, the arrivals of L, $3L$, $5L$,... have the same polarity while the $2LS$ and $2LS'$ modes are of opposite polarity compared to the $L\,2S$ and $L\,2S'$ modes. This occurs because on reflection at a free surface, a wave changes its polarity. (v) For epicentral and near-epicentral waveforms, there are strong similarities between the signals immediately following the arrivals of multiply reflected longitudinal modes. Such similarities can often also be observed in the off-epicentral waveforms, following, say, the $5L$, $7L$, $9L$, $11L$, etc. modes. Before and around the arrival of a $3L$ mode, the off-epicentral signals include the effects of S, S', H (head wave) modes which may die out quickly as the signals propagate farther. Consequently, there is little similarity in the signals following the L and $3L$ modes with those following the other multiply reflected L modes. (vi) Knowledge of the theoretical Green's functions as shown in Figs. 4 and 5 assists in identifying the various modes, particularly when they are closely spaced or otherwise difficult to identify.

In all the detected signals described in the following sections, the arrival time t_l of the first longitudinal mode (L) was identified as the point at which the signal amplitude suddenly rises above the noise level. Differences between the arrival times of the L and the multiply reflected longitudinal modes ($3L$,$5L$,$7L$,...) were determined from the velocity curve by measuring the times between the sharp peaks. Although these occur shortly after the arrivals of these modes, since time intervals were measured, the errors in the calculation of the wave speeds are thought to be negligible.

A. Isotropic media

An epicentral waveform generated by a glass capillary fracture and detected by the capacitive transducer is shown in Fig. 6. The specimen was a soda-lime glass plate of thickness 0.962 cm. When this signal is differentiated with respect to time to obtain the velocity signal, the arrivals of various wave modes become clearly identifiable, similar to the im-

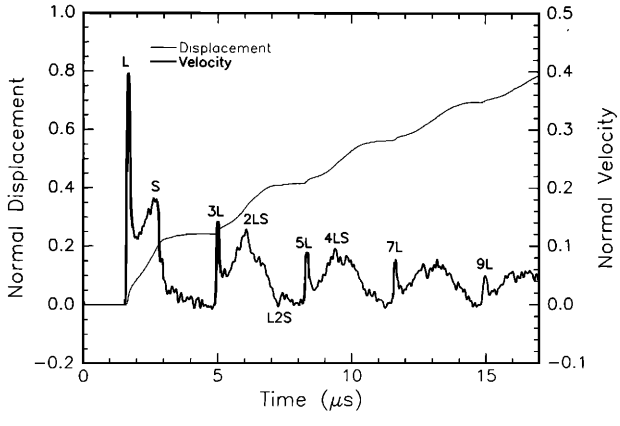

FIG. 6. Epicentral displacements and velocity signals obtained with a capillary fracture source and a capacitive transducer. Soda-lime glass plate specimen.

pulse response shown in Fig. 4. Denoting the thickness of the plate by h, one derives the longitudinal wave speed

$$V_l = (n-1)h/(t_{nl} - t_l). \tag{17}$$

For determination of the shear wave speed, we make use of the arrival of the L $2S$ mode instead of the S or the $2LS$ mode, provided that the L $2S$ mode is clearly identifiable as shown in Fig. 6. With this procedure, one minimizes the error associated with the calculated shear wave speed. The shear wave speed is given by

$$V_s = 2h/(t_{l2s} - t_l). \tag{18}$$

The longitudinal and shear wave speeds of glass calculated using the arrivals of L, L $2S$, and $7L$ modes and Eqs. (17) and (18) are

$$V_l = 0.579 \text{ cm}/\mu\text{s} \quad \text{and} \quad V_s = 0.340 \text{ cm}/\mu\text{s}.$$

For an off-epicentral receiver located at $r = qh$ from the epicenter of an elastically isotropic plate, one can choose any combination of three arrivals of L, S, nL, $2LS$, and head wave modes. For detection of the head wave, the receiver position r should be greater than $h\tan[\sin^{-1}(V_s/V_l)]$. This corresponds to a distance of 0.738 cm for the aluminum alloy plate specimen whose thickness was 1.288 cm. If one chooses the L, S, and nL modes, then V_l and V_s are obtained from the following relations

$$V_l = \frac{[(n^2+q^2)^{1/2} - (1+q^2)^{1/2}]}{t_{nl} - t_l}, \tag{19}$$

$$\frac{1}{V_s} = \frac{1}{V_l} + \frac{t_s - t_l}{(1+q^2)^{1/2}h}. \tag{20}$$

Similarly, measurement of the arrivals of the L, $3L$, and H modes can be used to obtain an additional equation relating the wave speeds. That is,

$$t_h - t_l = \frac{h}{V_l}\left(q - (1+q^2)^{1/2} - \frac{V_s}{(V_l^2 - V_s^2)^{1/2}} + \frac{V_l^2}{V_s(V_l^2 - V_s^2)^{1/2}}\right). \tag{21}$$

The determination of both V_l and V_s from Eqs. (19)–(21) is straightforward once the data of t_l, t_s, and t_h is known.

The off-epicentral waveform shown in Fig. 7 was detected in an isotropic, polycrystalline aluminum alloy plate of thickness $h = 1.288$ cm at a receiver position $r = 1.836h$ ($= 2.4$ cm) from a pulsed laser source. The thermoelastic expansion resulting from the deposition of the laser's energy gives rise to a large horizontal dipole force which generates strong longitudinal wave modes along the surface. These continuously shed head waves into the interior of the specimen which can be detected by a receiving transducer. Referring to Fig. 5 and recalling that the piezoelectric signal approximately resembles a velocity signal, the arrivals of various wave modes can be identified as in Fig. 7. From the arrival time data of t_l, t_s, t_{3l}, and t_h, one obtains from Eqs. (19) and (20)

$$V_l = 0.627 \text{ cm}/\mu\text{s} \quad \text{and} \quad V_s = 0.310 \text{ cm}/\mu\text{s}.$$

An identical result is obtained using Eqs. (19) and (21). Using the arrivals of $2LS$ and other two modes also yields

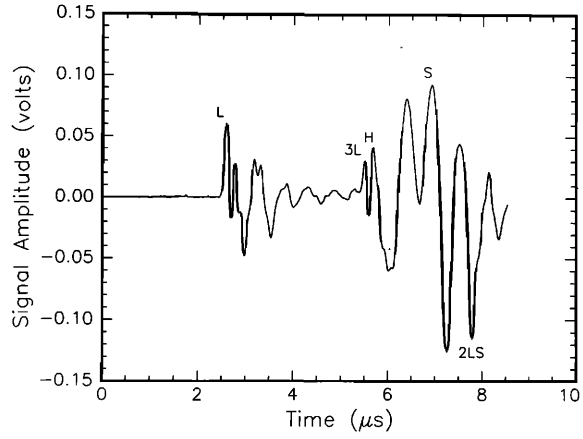

FIG. 7. Signal detected by a piezoelectric transducer at a 24-mm positions from epicenter using a 12.88-mm-thick Al plate and a laser beam source.

nearly identical results. It was also found that both V_l and V_s could be determined from the arrivals of L, S, $3L$, $5L$, and etc. which were identified in the off-epicentral signals from a capillary fracture source. The arrival of head waves could not be detected in the signals from the capillary fracture source because this source generates relatively weak horizontal displacements. The off-epicentral signals resulting from a capillary fracture source are not shown.

B. Silicon cubic single crystals

1. Epicentral waveforms

Measurements were made on three, disk-shaped specimens of single crystals of silicon. The normals to the surface of the disks were oriented along the ⟨100⟩, ⟨101⟩, or ⟨111⟩ directions as illustrated in Fig. 1. The diameter of the Si crystals were 7.62 cm and approximately 1 cm in thickness. In Figs. 8–10 are shown the epicentral displacement signals generated by capillary fractures and detected by the capacitive transducer. The time derivatives of the signals (corresponding to the velocity) are also shown. We note the strong resemblence between these displacement waveforms and the epicentral signal for an isotropic plate shown in Fig. 4. Because the theoretical Green's functions for an anisotropic media are not yet available, we apply the knowledge obtained from the isotropic case to provide guidance in identifying the various wave arrivals in the waveforms of the anisotropic specimens.

However, as shown in Fig. 8(a), the epicentral response of a ⟨100⟩-oriented crystal exhibits an unexpected behavior. The arrival of the first longitudinal wave (L) mode causes a sharp rise in normal surface displacement, which is quickly followed by a plateau, completely unlike the waveforms of isotropic media. This is followed by a surprisingly large "dip" which corresponds to the arrival of the first (fast) shear mode. This feature is also completely absent in signals detected in isotropic media. The 1-mm-diam capacitive transducer which was used to detect these signals subtends an angle of 5.8° viewed from the excitation point. Referring to the wave surface shown in Fig. 2(b) in the vicinity of the

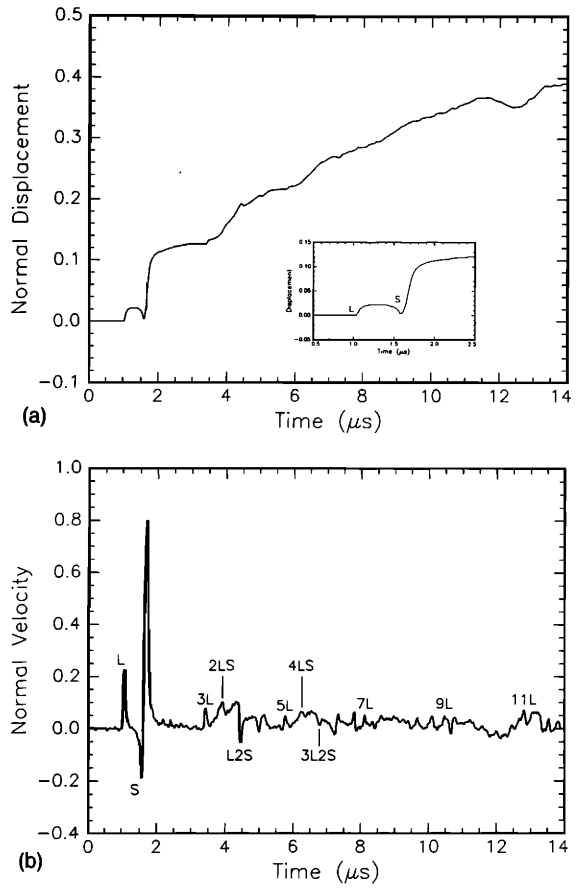

FIG. 8. Epicentral waveforms of a ⟨100⟩-oriented Si crystal obtained with capillary fracture source and capacitive transducer. (a) Normal displacement. (b) Velocity.

⟨100⟩ direction one can determine the range of group velocities for shear modes propagating within 2.9° of this direction. The range of arrival times of these two shear modes is calculated to be about 120 ns, which is approximately equal to the width of the dip. It thus appears that the arrival of the fastest shear mode is accompanied by a downward motion in

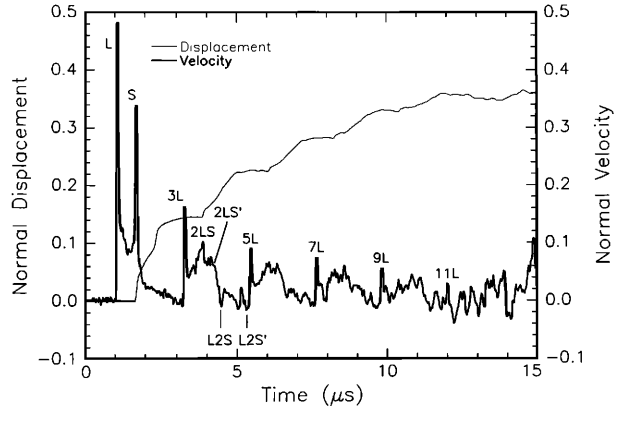

FIG. 9. Epicentral waveforms of a ⟨101⟩-oriented Si crystal obtained with a capillary fracture source and a capacitive transducer.

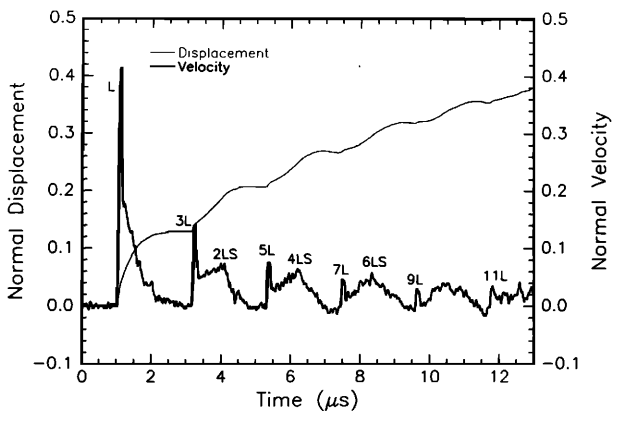

FIG. 10. Epicentral waveforms of a ⟨111⟩-oriented Si crystal obtained with capillary fracture source and capacitive transducer.

the normal displacement of the surface while the arrival of the slowest shear mode restores positive surface velocity. A careful examination of the arrival times in the velocity curve of Fig. 8(b) and comparison with the phase velocities obtained by plane wave methods by others[55,56] as well as us, reveals that the minimum point denoted by S in the velocity signal corresponds very closely to the phase velocity of shear wave propagating in {100}-type directions.

One can clearly identify in the later portion of the waveforms the regularly spaced arrivals of the multiply reflected longitudinal modes. The arrival times of the L and $11L$ signals were used to calculate V_l. For a more accurate determination of the shear wave phase velocity, we used the arrival of the L $2S$ signal rather than the S signal. The wave speeds determined in a ⟨100⟩ direction of a single crystal of silicon are

$$V_l = 0.843 \text{ cm}/\mu\text{s} \quad \text{and} \quad V_s = 0.580 \text{ cm}/\mu\text{s}.$$

The shear motions generated by the glass capillary fracture source in a ⟨101⟩-oriented crystal specimen results principally in the fast shear mode whose particle displacements are in the ⟨010⟩ direction. This wave is directly related to the elastic constant C_{44}. The first arrival of the slow shear mode (S') whose particle displacements are in the $\langle 10\bar{1} \rangle$ direction is related to the elastic constant C_s', but this does not appear in the velocity signal shown in Fig. 9. When the first longitudinal mode (L) reflects on the bottom surface, it is converted into longitudinal ($2L$), fast shear (LS), and slow shear (LS') modes. These travel back to the top surface, whereupon the $2L$ mode is reflected and mode-converted into longitudinal ($3L$), fast shear ($2LS$), and slow shear ($2LS'$) modes. These are the signals detected by the transducer at the bottom surface. After reflection at the top surface, the LS and LS' modes are converted into fast shear (L $2S$) and slow shear (L $2S'$) modes, respectively, which also appear in the signal detected on the bottom surface. One can also identify the arrivals of $5L$, $4LS$, $4LS'$, $3L$ $2S$, $3L$ $2S'$, and so on, even though the arrivals of these modes become less distinct as the waves propagate farther in the material and are attenuated. One may be inclined to assign the local minimum point found between the L $2S$ and L $2S'$ arrivals as

the arrival of the $L\,2S'$ mode. However, this is not the case because the time interval between the arrivals of the identified $3L$ and $L\,2S'$ modes is twice the difference between the arrival times of $3L$ and $2LS'$ as expected. The $L\,2S'$ signal arrives just prior to that of the $5L$ signal because the wave speed V_s' is slightly greater than 0.5 V_l. Again, the arrivals of L, $11L$, $L\,2S$, and $L\,2S'$ (but not the S) signals were used to calculate the wave speeds in the ⟨101⟩ direction

$$V_l = 0.914 \text{ cm}/\mu\text{s}, \quad V_s = 0.581 \text{ cm}/\mu\text{s},$$

and

$$V_s' = 0.467 \text{ cm}/\mu\text{s}.$$

We note that the velocity of the shear wave V_s obtained in the ⟨101⟩-oriented crystal is nearly identical with that obtained using a ⟨100⟩-oriented crystal.

The velocity waveform shown in Fig. 10 was obtained on a ⟨111⟩-oriented crystal with the capillary fracture source. There appears to be no appreciable shear mode signal. Furthermore, the $L\,2S$ and $3L\,2S$ modes, etc., are also missing. However, the multiply reflected longitudinal modes are quite pronounced with the $2LS$, $4LS$, and $6LS$ modes identified in the figure, although the exact arrivals of some of these are somewhat difficult to locate because of the noise. Measurement of the arrival times of L, $11L$, and $2LS$ yield for the wave speeds in the ⟨111⟩ direction

$$V_l = 0.935 \text{ cm}/\mu\text{s} \quad \text{and} \quad V_s = 0.498 \text{ cm}/\mu\text{s}. \qquad (22)$$

Because of the uncertainties associated with the determination of the $2LS$ arrival and a relatively small difference between t_{2ls} and t_{3l}, the value of V_s found by such measurements may have an error as high as 5%. As noted earlier, the shear wave propagating in the ⟨111⟩ direction does not have its wave normal in that direction and so the procedure for extracting an elastic constant from this measurement is not straightforward.

It is noted that the measurements made on signals generated by the capillary fracture source and detected with the piezoelectric transducer were not as successful for the three crystal orientations as those made on signals detected with the capacitive transducer. In the piezoelectric transducer signals, only the speed of the longitudinal modes could be measured with reasonably good accuracy, but the results were never better than those made from capacitive transducer detected signals. The other wave modes, such as S, S', $2LS$, $2LS'$, $L\,2S$, and $L\,2S'$ were, in general, very difficult to identify in the signals that had been detected with the piezoelectric transducer and in some cases could not be found at all. In an attempt to circumvent this difficulty, the use of a pulsed laser operating as a thermoelastic source was explored with the ⟨101⟩-oriented crystal specimen. The epicentral signal detected by the piezoelectric sensor is shown in Fig. 11. The laser source induces much stronger shear motion in the epicentral direction because the thermal expansions accompanying the deposition of laser photon energy results in a stronger horizontal excitation as mentioned earlier. Unfortunately, the detection of laser-generated signals by the capacitive transducer was not successful because of its lower sensitivity. The only alternative was to increase the intensity of the laser excitation, but this was ruled out to

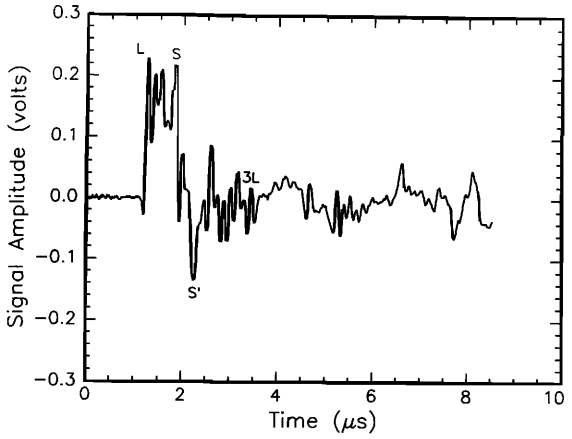

FIG. 11. Epicentral waveform of a ⟨101⟩-oriented Si crystal obtained with a pulsed laser source and detected with a piezoelectric transducer.

avoid ablation damage to the surface of the specimens. Figure 11 is a sample result with the arrivals of the L, S, S', and $3L$ modes indicated. The arrivals of the other modes are difficult to identify. The arrival of the $3L$ mode was determined by recognizing similarities in the signal between the arrivals of the L and the S modes with the signal following the $3L$ arrival. From the arrival times of the L, S, S' and $3L$ modes, one finds

$$V_l = 0.913 \text{ cm}/\mu\text{s}, \quad V_s = 0.572 \text{ cm}/\mu\text{s},$$

and

$$V_s' = 0.467 \text{ cm}/\mu\text{s}.$$

However, since the time intervals between arrivals of the modes used for the calculation of the above wave speeds are smaller than those for the modes used in the displacement transducer signal from the capillary source, the above results will likely have larger errors.

In summary, epicentral signals yield very precise longitudinal wave speeds with accuracies approaching 0.3%, which can be improved by using a waveform digitization rate higher than that used in the present study. If three crystals of ⟨100⟩, ⟨110⟩, and ⟨111⟩ orientations are available with nearly identical elastic moduli, accurate values of three longitudinal wave speeds in each of these directions can be determined. However, these three longitudinal wave speeds are not sufficient to determine the values of the three elastic constants of the material since the formulas relating the longitudinal wave speeds to elastic constants in the ⟨100⟩, ⟨110⟩, and ⟨111⟩ directions in a cubic material are not independent of each other (recall Table I). At least one additional shear wave speed is needed to determine the three elastic constants. For the measurement of the wave speed of a fast shear mode associated with the elastic constant C_{44}, either {100}- or {110}-type oriented crystals can be used, with either one yielding virtually the same accuracy. However, as the present study has shown, one should pay particular attention when making measurements in a {100}-type crystal whose epicentral signal exhibits the unusual behavior at the arrivals of shear modes with a range of group velocities. Clearly, if one wishes to determine all three wave speeds as accurately

as possible so that all three elastic constants of the material can be determined from a single epicentral waveform, one should use a {110}-type oriented crystal with a capillary fracture source and a capacitive sensor to detect the signals.

2. Off-epicentral waveforms

The determination of three wave speeds for waves propagating in an arbitrary off-epicentral direction is difficult for several reasons. The governing Christoffel equations relating wave speeds and elastic constants are complicated functions relating the wave speeds, elastic constants and propagation direction. Reflection and mode conversion of the waves at the free surfaces complicate matters. As a result, the identification of various modes in the received signals is difficult. For this reason, we focus here only on the simplest case, namely, the off-epicentral signals detected in ⟨100⟩- and ⟨101⟩-oriented crystals by a sensor located in a {110}-type direction from the excitation source. For a ⟨111⟩-oriented crystal, which has a threefold symmetry, the reflection and mode conversion of rays propagating in off-epicentral directions is extremely complicated and will not be treated here. The governing equations relating the wave speeds and the elastic constants for a ⟨100⟩-oriented crystal are Eqs. (4)–(6) while for a ⟨101⟩-oriented crystal, Eq. (14) also applies.

Figure 12 shows the velocity signal obtained from a displacement signal detected by a capacitive transducer located a distance of $\sqrt{3}h$ from epicenter in a $\langle 1\bar{1}0\rangle$ direction from the source in a ⟨101⟩-oriented crystal whose thickness h was 0.997 cm. In Fig. 13 is the signal detected by a piezoelectric transducer situated in a ⟨110⟩ direction at a $1h$ ($h = 0.991$ cm) unit away from epicenter of a ⟨100⟩-oriented crystal. The arrivals of various modes are identified in both figures. The signals in both of the above examples were generated by a capillary fracture. It is seen in Fig. 12 that the arrival of the $3L$ mode is before the S' mode. Both the S' as well as the S modes appear in the waveforms as negative peaks. In the signal shown in Fig. 13, both the S and the S' modes also appear as negative peaks arriving prior to the $3L$ mode. One can readily identify in the waveform shown in Fig. 13 the positive peaks following the arrivals of the $7L$, $9L$, $11L$ modes. A similar pattern of ray arrivals is present in the off-epicentral signals obtained with isotropic plates (which are not shown here). It should be noted that the signals generated by monopolar and dipolar sources decrease with their travel distance from these sources according to R^{-1} and R^{-2}, respectively. As a result, the pattern of ray arrivals may be difficult to observe in the signals generated by a relatively weak dipolar excitation such as the pulsed laser source. We note also that in the off-epicentral waveforms, the arrivals of the $3L$, $5L$, $7L$, $9L$, and $11L$ modes are more or less regularly spaced. This is probably a consequence of the small differences between wave speeds of the longitudinal modes and the roughly equal increments in acoustic path length between them.

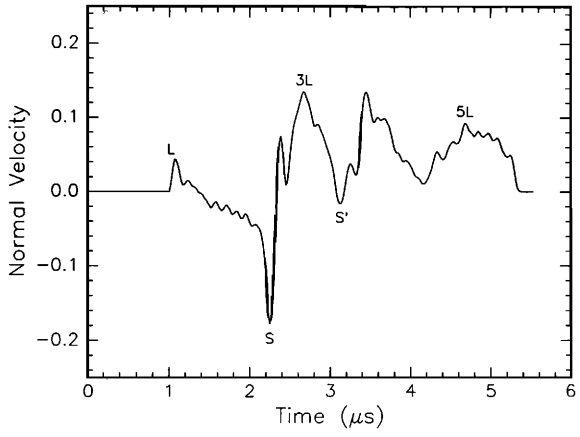

FIG. 12. Off-epicentral velocity signal of a ⟨101⟩-oriented Si crystal obtained with a capillary fracture source and a capacitive transducer located in a $\langle 1\bar{1}0\rangle$ direction from the source.

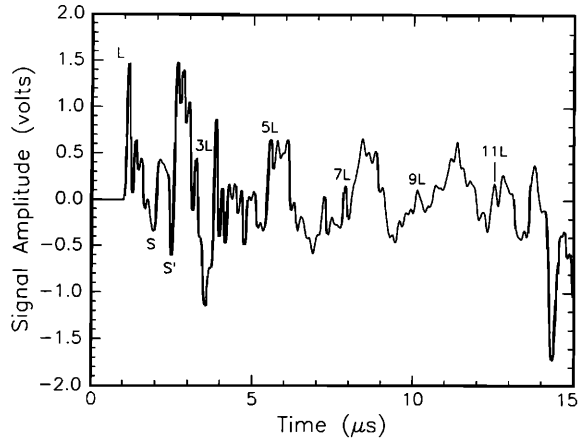

FIG. 13. Off-epicentral signal of a ⟨100⟩-oriented Si crystal obtained with a capillary fracture and a piezoelectric transducer located in a ⟨110⟩ direction from the source.

The arrivals of L, S, S', and one (nL) of the multiply reflected longitudinal modes can be used to determine the three wave speeds. Choosing two or more multiply reflected longitudinal modes leads to a larger error because of small differences between their wave speeds. Using a set of differences in arrival times of these modes, one can form three nonlinear simultaneous equations for the three wave speeds. The propagation directions of L, S, and S' modes are all those of {101}-type and hence one can make use of Eqs. (12a)–(12c) to reduce these three equations to one equation of one variable. To simplify the equations, the density ρ is here arbitrarily set to unity since it cancels in the final result of the wave speed calculation. Let

$$\zeta_s' \equiv 1/V_s' = 1/\sqrt{C_s'} \tag{23a}$$

and

$$\zeta_s \equiv 1/V_s = 1/\sqrt{C_{44}}, \tag{23b}$$

and

$$\tau_1 \equiv (t_s' - t_s)/p_{[110]} \tag{24a}$$

and

$$\tau_2 \equiv (t'_s - t_l)/p_{[110]}, \tag{24b}$$

where $p_{[110]}$ is the acoustic path length which the L, S, and S' modes have traveled from the source to the receiver. The quantity $p_{[110]}$ is equal to $\sqrt{2}h$ for a ⟨100⟩-oriented crystal and to $2h$ for a ⟨101⟩-oriented crystal. The above equations can be rewritten to obtain the expressions for the elastic constants

$$C'_s = V'^2_s = \zeta'^{-2}_s, \tag{25a}$$

$$C_{44} = V_s^2 = (\zeta'_s - \tau_1)^{-2}, \tag{25b}$$

$$C_{11} = V_l^2 = \zeta'^{-2}_s - (\zeta'_s - \tau_1)^{-2} + (\zeta'_s - \tau_2)^{-2}. \tag{25c}$$

Equations (25a)–(25c) permit us to express C_{11}, C_{44}, and C'_s in terms of a single variable ζ'_s. We write similarly

$$\tau_3 = t_{nl} - t'_s = \frac{p_{nl}}{V_{nl}} - \frac{p_{[110]}}{V'_s}, \tag{26}$$

where p_{nl} is the acoustic path of the nL mode which, in propagating from source to receiver, has traveled n times between the opposite faces of the crystal specimen. For a ⟨100⟩-oriented crystal, one obtains

$$p_{nl} = (n^2 + 1)^{1/2}h \tag{27a}$$

and

$$\tan\phi = 1/n \tag{27b}$$

and for a ⟨101⟩-oriented crystal

$$p_{nl} = (n^2 + 3)^{1/2}h. \tag{28}$$

The angle ϕ in Eq. (27b) was previously defined in Eqs. (5) and (6). A formula for V_{nl} can be found from Eq. (5) for a ⟨100⟩-oriented crystal in a direction of angle ϕ and from Eq. (14) for a ⟨101⟩-oriented crystal in a direction specified by n_{12}. Substituting Eqs. (27) and (28) for a ⟨100⟩- and a ⟨101⟩-oriented crystal, respectively, into Eq. (26) and expressing C_{11}, C_{44}, and C'_s in terms of the single variable ζ'_s, one obtains a nonlinear equation of terms of this variable. This equation was solved using the "Find Root" program of *Mathematica*.[54] Using only the real, positive root of ζ'_s, the three wave speeds were calculated according to Eqs. (25a)–(25c).

The three wave speeds obtained from the arrivals of L, S, S', and $3L$ modes in a ⟨101⟩-oriented crystal are

$$V_l = (C_{11}/\rho)^{1/2} = 0.834 \text{ cm}/\mu\text{s},$$

$$V_s = (C_{44}/\rho)^{1/2} = 0.580 \text{ cm}/\mu\text{s},$$

and

$$V'_s = (C'_s/\rho)^{1/2} = 0.462 \text{ cm}/\mu\text{s},$$

and using, for example, the arrivals of the L, S, S' and $5L$ modes yields

$$V_l = (C_{11}/\rho)^{1/2} = 0.833 \text{ cm}/\mu\text{s},$$

$$V_s = (C_{44}/\rho)^{1/2} = 0.580 \text{ cm}/\mu\text{s},$$

and

$$V'_s = (C'_s/\rho)^{1/2} = 0.461 \text{ cm}/\mu\text{s}.$$

Similarly in the waveforms of a ⟨100⟩-oriented crystal, if one selects the arrivals of the L, S, S', and $7L$ modes, one obtains for the wave speeds

$$V_l = (C_{11}/\rho)^{1/2} = 0.841 \text{ cm}/\mu\text{s},$$

$$V_s = (C_{44}/\rho)^{1/2} = 0.574 \text{ cm}/\mu\text{s},$$

and

$$V'_s = (C'_s/\rho)^{1/2} = 0.467 \text{ cm}/\mu\text{s}.$$

Using other multiply reflected longitudinal modes instead of the $7L$ signal resulted in wave-speed values which were identical within an experimental error. It is noted that the wave speeds obtained from off-epicentral waveforms compare very well with those determined from epicentral signals. However, we believe that measurements on off-epicentral waveforms have greater experimental errors because of transducer aperture effects. Also contributing to the error are difficulties related to the precise positioning of the detector in a {101}-type direction relative to the excitation source.

Table II lists the values of three elastic constants C_{11}, C_{44}, and C'_s, of silicon, where $C'_s \equiv (1/2)(C_{11} - C_{12})$, which have been obtained in the present study and those obtained by others previously.[55,56] It is noted that although the prior work utilized different experimental techniques, the agreement with the values reported here is, in all cases, within ~1%. The small differences between the measurements reported here and the previous work can likely be attributed to slight differences in the single-crystal specimens.

III. SUMMARY AND CONCLUSIONS

We have demonstrated in this paper several procedures for determining the wave speeds of ultrasonic waves in both isotropic and anisotropic specimens. The procedures assume that the propagating medium is nondispersive and that the differences between the phase and group velocities are negligible in the propagation directions considered. It was demonstrated that the longitudinal wave speed can be accurately determined from epicentral waveforms. With a ⟨110⟩-oriented crystal, values of all three elastic constants can be accurately determined from just one epicentral waveform. This method has advantages in that one can avoid possible errors resulting from making measurements on several specimens of different orientations which may have slightly

TABLE II. Elastic constants of single-crystal silicon. The asterisk indicates $C'_s \equiv (C_{11} - C_{12})/2$.

References	Method	C_{11} [GPa]	C_{44} [GPa]	C'^*_s [GPa]
This work	a	166.8	78.7	50.9
This work	b	167.1	78.7	50.9
Ref. 46	c	165.7	79.5	50.9
Ref. 47	d	165.7	79.4	51.0

[a] Obtained from epicentral waveforms of a ⟨101⟩ oriented crystal in this experiment.
[b] Obtained using the plane-wave broadband pulse technique.
[c] Obtained using the rf burst pulse echo technique.
[d] Obtained from determination of ultrasonic wavelengths.

differing elastic moduli. We have also shown that the three elastic constants can be obtained from one off-epicentral waveform detected by the sensor located in a {110}-type direction of either ⟨100⟩- or ⟨101⟩-oriented crystals. The determination of the three wave speeds using the waveforms detected by sensors located in general, off-epicentral directions from the source is, in principle, possible, provided that more than four distinct wave modes can be identified in a detected waveform. For those ray directions for which differences between group and phase velocities are significant, errors may arise in the determination of the phase velocities when measured group velocity data are treated as phase velocity data and hence the corresponding elastic constants will also be in error. This subject will be further discussed in a subsequent paper.

Based on the work described here, the following conclusions can be drawn.

(1) The wave speed of longitudinal waves propagating in an epicentral direction can be precisely determined from the arrivals of L and multiply reflected longitudinal modes.

(2) An accurate determination of the shear wave speeds can be obtained from measurement of the arrivals of L, $L\,2S$, and $L\,2S'$ modes in the detected epicentral signals. In a ⟨101⟩-oriented crystal, one can observe signals corresponding to the mode converted modes, $L\,2S$ and $L\,2S'$.

(3) Determination of the wave speeds from off-epicentral waveforms, whether the propagating medium is isotropic or not, can be achieved by identifying the arrivals of various wave modes, such as L, S, S', H, and $3L$, $5L$, $2LS$, $L\,2S$, and so on.

(4) The values of the three wave speeds and hence the three elastic constants of a cubic single crystal can be determined from a single waveform detected by sensors situated in {101}-type directions whether they are epicentral or not. The epicentral waveform yields the most accurate determination.

(5) Because of differing group velocities associated with the various shear modes propagating close to {100}-type directions, the epicentral displacement signal generated in a ⟨100⟩-oriented crystal by a glass capillary fracture source exhibits an unexpected behavior at the shear wave arrivals. Coinciding with these arrivals is a sharp dip in the displacement curve. It appears that the phase velocity of shear wave propagating in a ⟨100⟩ direction corresponds to a point of sharp negative minimum in the velocity signal.

(6) A capillary fracture source generates little shear motion in waves propagating in an epicentral direction in a ⟨111⟩-oriented crystal. Nor does it generate any appreciable slow shear (S') mode propagating in an epicentral direction in a ⟨101⟩-oriented crystal.

(7) A pulsed laser excitation induces a strong horizontal displacement on the surface. As a result, this source is well suited for measurement of the wave speeds of the shear modes propagating in an epicentral direction. This source is also useful for generating head waves whose detection by an off-epicentral sensor might be used to determine the wave speeds with higher accuracy.

(8) Differences between the group and phase velocities of the signal should be considered when determining the wave speeds and the elastic moduli of an anisotropic solid from waveforms generated by a broadband, point excitation.

ACKNOWLEDGMENTS

The authors thank Mrs. Lin Niu for carrying out some of the preliminary calculations. Financial support of the Office of Naval Research (Physical Acoustics Program) and the National Science Foundation through the Materials Science Center at Cornell University is greatly appreciated.

[1] R. L. Forgacs, "An improved sing around system for ultrasonic velocity measurements," IRE Trans. Instrum. **I-9**, 359–367 (1960).
[2] J. Williams and J. Lamb, "On the measurement of ultrasonic velocity in solids," J. Acoust. Soc. Am. **30**, 308–313 (1958).
[3] H. J. McSkimin, "Pulse superposition method for measuring ultrasonic wave velocities in solids," J. Acoust. Soc. Am. **33**, 12–16 (1960).
[4] E. P. Papadakis, "Ultrasonic attenuation and velocity in three transformation products in steel," J. Appl. Phys. **35**, 1474–1482 (1964).
[5] D. I. Bolef and J. deKlerk, "Some continuous-wave techniques for the measurement of velocity and attenuation of ultrasonic waves between 1 and 1000 mc," IEEE Trans. Ultrasonic Eng. **UE-10**, 19–26 (1963).
[6] R. G. Leisure and R. W. Moss, "A continuous wave technique for the automatic measurement of ultrasonic velocity charges," Rev. Sci. Instrum. **40**, 946–948 (1969).
[7] D. I. Bolef and M. Menes, "Measurement of elastic constants of RbBr, RbI, CsBr and CsI by an ultrasonic resonance technique," J. Appl. Phys. **31**, 1010–1017 (1960).
[8] M. S. Conradi, J. G. Miller, and J. S. Heyman, "A transmission oscillator ultrasonic spectrometer," Rev. Sci. Instrum. **45**, 358–360 (1974).
[9] R. Truell, C. Elbaum, and B. Chick, *Ultrasonic Methods in Solid State Physics* (Academic, New York, 1969), pp. 78–87.
[10] E. P. Papadakis, "Ultrasonic velocity and attenuation: Measurement methods with scientific and industrial applications," in *Physical Acoustics*, edited by W. P. Mason and R. N. Thurston (Academic, New York, 1976), Vol. XII, Chap. 5, pp. 277–374.
[11] M. A. Breazeale, J. H. Cantrell, Jr., and J. S. Heyman, "Ultrasonic wave velocity and attenuation measurements," in *Methods of Experimental Physics*, edited by P. D. Edmonds (Academic, New York, 1981), Vol. 19, Chap. 2, pp. 67–135.
[12] W. Sachse and K. Y. Kim, "Point-source/point-receiver materials testing," in *Review of Progress in Quantitative Evaluation*, edited by D. O. Thompson and D. E. Chimenti (Plenum, New York, 1987), Vol. 6A, pp. 311–320.
[13] F. R. Breckenridge, C. E. Tschiegg, and M. Greenspan, "Acoustic emission: some applications of Lamb's problem," J. Acoust. Soc. Am. **57**, 626–631 (1975).
[14] N. N. Hsu, "Acoustic emissions simulator," U. S. Patent 4,018,084 assigned to Lockheed Aircraft Corp., Burbank, CA (May, 1976).
[15] C. B. Scruby, R. J. Dewhurst, D. H. Hutchins, and S. B. Palmer, "Laser generation of ultrasound in metals," in *Research Techniques in Nondestructive Testing*, edited by R. S. Sharpe (Academic, London, 1982), Vol. 5, pp. 281–327.
[16] G. S. Cargill, "Electron-acoustic microscopy," Phys. Today, **34**(10), 27–32 (1981).
[17] K. Y. Kim and W. Sachse, "X-Ray generated ultrasound," Appl. Phys. Lett. **43**, 1099–1101 (1983).
[18] W. Sachse, "Transducer considerations for point-source/point-receiver materials measurements," in *Ultrasonic International '87 Conference Proceedings* (Butterworth Scientific, Guildford, Surrey, UK, 1987), pp. 419–425.
[19] W. Sachse and K. Y. Kim. "Quantitative acoustic emission and failure mechanics of composite materials," Ultrasonics **25**, 195–203 (1987).
[20] N. N. Hsu and D. G. Eitzen, "Point source/point receiver ultrasonic wave speed measurement," in *Ultrasonic International '87 Conference Proceedings* (Butterworth Scientific, Guildford, Surrey, UK, 1987), pp. 509–513.
[21] J. D. Aussel and J.-P. Monchalin, "Precision laser-ultrasonic velocity measurement and elastic constant determination," Ultrasonics, **27**, 165–177 (1989).

[22] J.-P. Monchalin, R. Héron, and N. Muzak, "Heterodyne interferometric laser probe to measure continuous ultrasonic displacements," Rev. Sci. Intrum. **56**, 543–546 (1985).
[23] R. J. Dewhurst, C. Edwards, A. D. W. Mckie, and S. B. Palmer, "Remote laser system for ultrasonic velocity measurement at high temperatures," J. Appl. Phys. **63**, 1225–1227 (1988).
[24] C. A. Calder, E. C. Draney, and W. W. Wilcox, "Noncontact measurement of the elastic constants of plutonium at elevated temperature," J. Nucl. Mater. **27**, 126–136 (1981).
[25] L. Piché, B. Champagne, and J.-P. Monchalin, "Laser ultrasonics measurements of elastic constants of composites," Mater. Eval. **45**, 74–79 (1987).
[26] B. Castagnède, W. Sachse, and M. O. Thompson, "Determination of the elastic constants of anisotropic materials via laser-generated ultrasound," in *Ultrasonic International '89: Conference Proceedings* (Butterworth Scientific, Ltd., Guildford, Surrey, UK, 1989), pp. 71–77.
[27] B. Castagnède, J. T. Jenkins, W. Sachse, and S. Baste, "Optimal determination of the elastic constants of composite materials from ultrasonic wavespeed measurements," J. Appl. Phys. **67**(6), 2753–2761 (1990).
[28] B. Castagnède, K. Y. Kim, W. Sachse, and M. O. Thompson, "Determination of the elastic constants of anisotropic materials using laser-generated ultrasonic signals," J. Appl. Phys. **70**(1), 150–157 (1991).
[29] J. D. Achenbach, *Wave Propagation in Elastic Solids* (North-Holland and Elsevier Science, Amsterdam, 1973).
[30] L. Knopoff, "Surface motions of thick plates," J. Appl. Phys. **29**, 661–670 (1957).
[31] A. N. Ceranoglu and Y. H. Pao, "Propagation of elastic pulses and acoustic emission in a plate: Part I, Theory; Part II, Epicentral response; Part II, General Responses," ASME J. Appl. Mech. **48**, 125–147 (1981).
[32] N. N. Hsu, "Dynamic Green's Functions of an Infinite Plate—A Computer Program," NBS Report #NBSIR 85-3234 (1985).
[33] U. Schleichert, K. J. Langenberg, W. Arnold, and S. Fabbender, "A quantitative theory of laser-generated ultrasound," in *Review of Progress in Quantitative Nondestructive Evaluation*, edited by D. O. Thompson and D. E. Chimenti (Plenum, New York, 1989), Vol. 8A, pp. 489–496.
[34] R. Ludwig, D. Moore, and W. Lord, "A comparative study of analytical and numerical transient force excitations on an elastic half space," IEEE Trans. Ultrason. Ferroelectr. Freq. Control **36**, 342–350 (1989).
[35] R. L. Weaver, W. Sachse, and L. Niu, "Transient ultrasonic waves in a viscoelastic plate," J. Acoust. Soc. Am. **85**, 2255–2261 (1989).
[36] R. L. Weaver, W. Sachse, and L. Niu, "Transient ultrasonic waves in a viscoelastic plate: Applications to materials characterization," J. Acoust. Soc. Am. **85**, 2262–2267 (1989).
[37] G. F. D. Duff, "The Cauchy problem for elastic waves in an anisotropic medium," Philos. Trans. R. Soc. London **252**, 249–273 (1960).
[38] N. Cameron and G. Eason, "Wave propagation in an infinite transversely isotropic elastic solid," Q. J. Mech. App. Math. **20**, 23–40 (1967).
[39] C. T. Buchwald, "Elastic waves in anisotropic media," Proc. R. Soc. London, Ser. A **253**, 563–580 (1959).
[40] F. R. Yeatts, "Elastic radiation from a point force in an anisotropic medium," Phys. Rev. **B29**, 1674–1684 (1984).
[41] A. Tverdokhlebov and J. Rose, "On Green's functions for elastic waves in anisotropic media," J. Acoust. Soc. Am. **83**, 118–121 (1988).
[42] A. G. Every, "Ballistic phonons and the shape of the ray surface in cubic crystals," Phys. Rev. **B24**, 3456–3467 (1981).
[43] J. F. Nye, *Physical Properties of Crystals* (Oxford U. P., London, 1957).
[44] B. A. Auld, *Acoustic Fields and Waves in Solids* (Krieger, Malabar, FL, 1990), 2nd ed., Vol. 1, Chap. 7.
[45] M. J. P. Musgrave, *Crystal Acoustics* (Holden-Day, San Francisco, 1970).
[46] F. I. Fedorov, *Theory of Elastic Waves in Crystals* (Plenum, New York, 1968).
[47] D. M. Barnett, J. Lothe, K. Nishioka, and R. J. Asaro, "Elastic surface waves in anisotropic crystals: a simplified method for calculating Rayleigh velocities using dislocation theory," J. Phys. Fluids **3**, 1083–1096 (1973).
[48] A. G. Every, "General closed-form expressions for acoustic waves in elastically anisotropic solids," Phys. Rev. B **22**, 1746–1760 (1980).
[49] M. J. P. Musgrave, "On the propagation of elastic waves in aeolotropic media. II media of hexagonal symmetry," Proc. R. Soc. London, Ser. A **226**, 356–366 (1954).
[50] G. F. Miller and M. J. P. Musgrave, "On the propagation of elastic waves in aeolotropic media. III media of cubic symmetry," Proc. R. Soc. London, Ser. A **236**, 352–383 (1956).
[51] P. Chadwick and G. Smith, in *Mechanics of Solids: Rodney Hill 60th Anniversary Volume*, edited by H. G. Hopkins and N. J. Sewell (Pergamon, New York, 1982), pp. 47–100.
[52] K. Y. Kim, L. Niu, B. Castagnède, and W. Sachse, "Miniaturized capacitive transducer for detection of broadband ultrasonic displacement signals," Rev. Sci. Instrum. **60**, 2785–2788 (1989).
[53] K. Y. Kim and W. Sachse, "Study of brittle fracture by acoustic emission from indentation cracks," J. Appl. Phys. **65**, 4234–4244 (1989).
[54] S. Wolfram, *Mathematica* (Addison-Wesley, Redwood City, CA, 1988), Chap. 3.
[55] J. J. Hall, "Electronic effects in the elastic constants of *n*-type silicon," Phys. Rev. **161**, 756–761 (1967).
[56] H. J. McSkimin, "Measurement of elastic constants at low temperatures by means of ultrasonic wave—data for silicon and germanium single crystals, and for fused silica," J. Appl. Phys. **24**, 988–997 (1953).